Atomistic Molecular Dynamics Simulation of Stress Relaxation upon Cessation of Steady-State Uniaxial Elongational Flow

Vagelis A. Harmandaris, Vlasis G. Mavrantzas, and Doros N. Theodorou*

Department of Chemical Engineering University of Patras and Institute of Chemical Engineering and High-Temperature Chemical Processes, GR 26500 Patras, Greece

Received November 2, 1999; Revised Manuscript Received May 11, 2000

ABSTRACT: A new approach is presented for predicting the linear viscoelastic properties of a polymer melt through a series of molecular dynamics (MD) simulations of the relaxation of well-equilibrated, preoriented, strained configurations. Such strained configurations have been accumulated (Mavrantzas and Theodorou, 1998) by employing the end-bridging Monte Carlo (EBMC) algorithm in the presence of a small tensorial field α_{xx} which orients the chains. They are representative of a melt under conditions of steady-state, uniaxial elongational flow. In the dynamic studies presented in this work, the tensorial field α_{xx} is removed and the relaxation of the system back toward its field-free, equilibrium state is monitored with MD. All simulations are performed in the $NTL_x\sigma_{yy}\sigma_{zz}$ statistical ensemble (Yang et al., 1997), where the following variables are kept constant: the number of particles N, the temperature T, the length L_x of the simulation box in the direction of flow, and the average stress $(\sigma_{yy} + \sigma_{zz})/2$ in the other two (lateral) directions. The physical experiment modeled through these $NTL_x\sigma_{yy}\sigma_{zz}$ MD simulations is one of *stress relaxation upon cessation of a steady-state, uniaxial elongational flow*. The relaxation of the melt is quantified by monitoring the temporal evolution of the normal stress σ_{xx} in the x direction, of the volume V, and of certain descriptors of the short- and long-length scale conformation of chains. These include the diagonal components $\tilde{c}_{xx}$, $\tilde{c}_{yy}$, and $\tilde{c}_{zz}$ of the conformation tensor and the chain mean-square end-to-end distance $\langle R^2 \rangle$, all as functions of time t. Results for the aforementioned properties, accumulated as statistical averages over many initial configurations subjected to $NTL_x\sigma_{yy}\sigma_{zz}$ MD simulations, are presented for two PE melt systems, C_{24} and C_{78}, both of which have been studied extensively in the past. By invoking the Rouse model, analytical expressions are derived for the functions $\sigma_{xx}(t)$ and $\tilde{c}_{xx}(t)$ corresponding to the experiment simulated. By mapping the simulation results on these expressions, the longest relaxation times τ_R of the melts are extracted in excellent agreement with previous equilibrium computer experiments (Harmandaris et al., 1998). The stress relaxation modulus $G(t)$ is computed from the equilibrium shear stress autocorrelation function at short times and from the spectrum of relaxation times extracted by mapping the MD results on the Rouse model at long times, yielding consistent and physically meaningful results.

1. Introduction

The rheological properties of polymer melts are of fundamental interest to industry because they govern the response of the melts to flow fields applied under processing conditions. Despite significant advances in understanding the structural and thermodynamic properties of polymer systems, however, relatively little simulation work has been conducted to obtain a detailed microscopic understanding of the rheological behavior of polymers, particularly when the molecular length approaches or exceeds the characteristic molecular length for the formation of entanglements. The reason for this is that rheological properties are intimately related with the long-time dynamics of polymer systems; for systems consisting of long chains, therefore, brute force MD simulations, usually employed to equilibrate microscopic models of material systems and to track their temporal evolution, are of limited utility, as they can only track at most a few tens of nanoseconds out of a dynamical response which typically lasts from microseconds to seconds.

Molecular simulations have been used to probe the response of amorphous polymers to deformation since the mid-1980s. Using molecular mechanics, Theodorou and Suter[1] made a connection between stress–strain curves in the elastic regime and molecular-scale phenomena in a glassy polymer. A similar methodology was followed later by Argon et al.[2] to simulate plastic deformation in a polymer glass.

Brown, Clarke, and co-workers were the first to apply the MD method to study the yielding behavior of amorphous, united-atom PE systems constructed from a single "parent" chain.[3] They subjected the PE systems to uniaxial tension by changing the y component of the applied pressure tensor, P_{yy}, at a constant (high) rate (either 5 or 1 bar ps^{-1}).

Gao and Weiner[4-6] presented an investigation of the dynamic properties of deformed polymer systems in the rubbery regime. They subjected the simulation box to a constant-volume elongation at a high, constant rate ($\dot{\varepsilon} = 2.77 \times 10^{10}$ s^{-1}) along the x direction, using a constant-temperature MD algorithm. All simulations were performed using the freely jointed chain model. This work was followed by a study of the birefringence of the uniaxially stretched system and of the relaxation of the stress developed in response to the imposed continuous deformation of the simulation box at the monomer level.

More recently, Yang et al.[7,8] proposed a MD technique for the simulation of uniaxial tension and compression of model amorphous polymer systems; this technique is molecular dynamics in the $NTL_x\sigma_{yy}\sigma_{zz}$ statistical

* To whom correspondence should be addressed at the University of Patras. Telephone: +3061-997-398. Fax: +3061-993-255. E-mail: doros@sequoia.chemeng.upatras.gr.

ensemble. Model linear PE systems were simulated with the new technique near and below the glass transition temperature T_g, and good qualitative agreement with experimental data was reported.

In parallel, nonequilibrium molecular dynamics (NEMD) simulations have appeared,[9,10] aiming at simulating special types of flows, such as shear. The simulation of elongational flows presents particular difficulties for traditional NEMD techniques, due to the finite time requirement imposed by the contraction of the simulation cell normal to the direction of elongation. To overcome this problem, in a series of papers, Todd and Daivis[11,12] calculated the elongational viscosity by applying an oscillating elongational strain rate; more recently, the same researchers proposed a new method for simulating elongational flow in a two-dimensional atomic fluid, involving spatially and temporally periodic boundary conditions.[13]

NEMD simulations of steady-state shear flow can lead directly to the shear viscosity. Simulating low shear rates, comparable to those encountered in most processing operations, is certainly possible algorithmically; it is not very useful in practice, however, as the huge fluctuations in instantaneous stress (on the order of 1 MPa for typical model system sizes) make it impossible to resolve the average stress with which the system responds to flow. Subtraction techniques,[14,15] designed to resolve the nonequilibrium stress response from the fluctuations through comparison with equilibrium trajectories initiated at the same configurations, run into problems of trajectory divergence. A promising alternative approach for resolving the response of nonequilibrium systems at small driving forces is the transient time correlation function approach of Morris and Evans;[16] This approach has been applied successfully to shear and elongational flow[17] simulations of simple fluids and is only now being extended to polymers.

In practice, the problem of resolving signal from noise in low-strain-rate NEMD simulations has forced most existing NEMD investigations of flow into the regime of very high strain rates (in excess of 10^9 s^{-1}). There the average stress is high enough to be resolved from the fluctuations. For liquids with long relaxation times, such as polymer melts, however, two new severe problems arise. First, the Deborah number (ratio of dominant material relaxation time to the characteristic time of the flow) is much higher than 1, which means that the simulated flow is in a strongly nonlinear regime. Extremely important linear viscoelastic properties, such as the stress relaxation modulus and the zero-shear-rate viscosity, characteristic of the "Newtonian plateau" regime, are inaccessible by the NEMD simulation. Second, the mere attainment of steady-state conditions within the duration of a NEMD simulation initiated at an equilibrium configuration becomes problematic, as the relaxation time of the molecules may well exceed the duration of the simulation. These problems become more severe the longer the chains, as the relaxation time of the fluid increases sharply with chain length. It is thus understandable that NEMD simulations of flow of alkane fluids longer than C_{100} have never been performed.[18]

Accumulating autocorrelation functions in the course of *equilibrium* MD simulations and then integrating these functions according to the prescriptions given by the Green–Kubo formalism is, of course, a way to obtain transport coefficients in the linear regime. This approach has been applied for the estimation of the zero-shear viscosity of alkane liquids up to C_{16}.[19] Its implementation for longer-chain systems becomes prohibitive computationally due to the aforementioned large fluctuations in instantaneous stress; accumulating the tails of stress autocorrelation functions out to times commensurate with the relaxation time of a polymeric liquid, with sufficient accuracy to allow estimation of the zero-shear viscosity through Green–Kubo integration, is impossible with currently available computational means.

We have recently introduced a hierarchical simulation approach for getting at the linear viscoelastic properties of long-chain polymer melts.[20] This approach relies upon conducting equilibrium atomistic MD simulations, accumulating dynamical properties and time autocorrelation functions, and mapping these properties and autococorrelation functions onto the corresponding expressions given by an appropriate coarse-grained (mesoscopic) model of polymer dynamics. In this way, key parameters of the coarse-grained model can be estimated from the atomistic simulations and then used in the context of the coarse-grained model to calculate the desired rheological properties. We have applied this approach to a series of moderately polydisperse linear melts of oligomeric polyethylene (PE), containing chains ranging in length from C_{12} to C_{156}. An appropriate coarse-grained model of dynamics in this regime is the Rouse model.[21] We have accumulated time autocorrelation functions for the Rouse modes of the chains in the course of equilibrium atomistic MD runs of duration up to 30 ns and shown that, for chain lengths between C_{70} and C_{156}, the Rouse model with a chain length-independent friction factor provides an excellent description of the relaxation of the first few modes. Using this friction factor, the melt density, and the unperturbed mean square end-to-end distance, as obtained from the atomistic simulations, within the Rouse model expression for the zero-shear viscosity η_0, we have been able to obtain predictions for η_0 in excellent agreement with experimental data in this regime of chain lengths. Furthermore, the self-diffusivities D of chains, as predicted from atomistic MD, give an estimate of the friction factor that is fully consistent with that extracted from the autocorrelation functions of Rouse modes. Predicted D values were found to be in excellent agreement with experimental values for all chain lengths examined.[20] Conducting equilibrium MD simulations of oligomeric melts of sufficiently high molecular weight and mapping the results of these simulations onto the Rouse model has thus emerged as a pragmatic, computationally feasible way of estimating linear viscoelastic properties, at least in the unentangled melt regime. A similar methodology has been proposed independently by Mondello et al.[22]

The aim of this paper is to extend this hierarchical methodology to systems which are away from equilibrium. To this end, in the present paper, we conduct molecular dynamics simulations starting from a large ensemble of configurations *oriented* along the x direction and representing a melt under steady-state uniaxial elongational flow. We then observe the isothermal relaxation of these configurations to thermodynamic equilibrium, keeping their dimensions along the x direction constant and the average normal pressure in the y and z directions equal to the atmospheric pressure. That is, we simulate an experiment of stress relaxation

upon cessation of a steady-state uniaxial elongational flow. In the course of the MD simulations we track the temporal evolution of the ensemble-averaged stress and of the overall conformational characteristics of the chains. We develop analytical expressions for these quantities as functions of time by solving the Rouse model under the initial and boundary conditions corresponding to our atomistic computer experiment. By mapping our simulation results onto the Rouse analytical expressions, we determine the friction factor or, equivalently, the Rouse time τ_R. Finally, we compare this estimate against the estimate previously obtained from equilibrium MD.

Our computer experiments are designed to be conducted within the linear viscoelastic regime. For the generation of the initial oriented configurations we rely not on MD, but on a powerful Monte Carlo (MC) algorithm we have developed.[23−25] This algorithm, end-bridging Monte Carlo (EBMC), employs moves that modify the connectivity among polymer segments while preserving a prescribed (narrow) molecular weight distribution. It can thus equilibrate the long-length scale features of a polymer melt orders of magnitude more efficiently than MD or other MC methods, its relative efficiency increasing dramatically with increasing chain length.[25] Sampling oriented melts under conditions of steady-state elongational flow with this algorithm relies upon postulating that the free energy of such a melt is a function of density, temperature, and of a coarse-grained descriptor of the overall conformation of chains, which we call the conformation tensor, $\tilde{\mathbf{c}}$.[24] The partial derivatives of the free energy with respect to the elements of $\tilde{\mathbf{c}}$ define a thermodynamic field α, whose elements are physically analogous to Deborah numbers. Oriented configurations corresponding to steady-state uniaxial elongational flow, such as that encountered in fiber spinning, are sampled with EBMC under a prescribed value of α_{xx}, all other elements of α being zero. In the present work this value of α_{xx} is everywhere smaller than 1, to keep the computer experiments within the linear regime.

As already mentioned, calculating the stress tensor in polymer melts within the linear viscoelastic regime via the conventional virial theorem route is fraught with huge statistical error, owing to the large fluctuations exhibited by the instantaneous stress. In our previous work[24] we have proposed a thermodynamic expression for the stress tensor in terms of the tensors $\tilde{\mathbf{c}}$ and α, which is based directly on the free energy function described above and is subject to much less statistical uncertainty. Comparison of stress components calculated by this expression against estimates based on the virial theorem has led to excellent agreement under steady-state flow conditions.[24] Here we test our thermodynamic expression for the stress under transient conditions, for the first time. We show that it is in full agreement with, but subject to much less statistical noise than, the virial theorem, and we use it to track stress relaxation in our melts.

Specific objectives of this paper are (a) to obtain the Rouse time and the overall distribution of relaxation times by mapping atomistic simulations of stress relaxation, carried out under *transient* conditions in the *linear* viscoelastic regime, onto the Rouse model; (b) to compare these properties against the corresponding estimates based on past equilibrium MD simulations[20] and against experimental evidence, and thus check the internal consistency and reliability of our equilibrium and nonequilibrium hierarchical approaches to the prediction of linear viscoelastic properties of unentangled melts; (c) to test our thermodynamic expression for the stress tensor σ in terms of the conformation tensor $\tilde{\mathbf{c}}$ and the orienting field σ under transient, nonequilibrium conditions; (d) to extract, as best as possible, the stress relaxation modulus $G(t)$ from our simulation results.

The approach described in this paper overcomes several limitations of conventional NEMD simulations, as they have been applied in the past to polymer melts: (a) There is no strain rate imposed externally in the course of the dynamic simulation; the melt is allowed to relax *at its own pace*, and not forced into flow situations that are far removed from experimental and processing practice. (b) Initial oriented configurations are prepared with EBMC, not MD, under conditions corresponding to small-strain rate, steady-state elongational flow. EBMC is much more efficient than MD in equilibrating properties which depend on structure at the length scale of entire chains. It thus yields a well-defined ensemble of preoriented configurations, no matter how long the chains or how weak the orienting fields are. The use of weak orienting fields ensures that the whole relaxation experiment is conducted within the linear viscoelastic regime. (c) Stress is calculated from the overall chain conformation via a free energy-based expression which affords excellent signal-to-noise ratio. Stresses based on this expression are found to be fully consistent with average stresses from the molecular virial theorem, to the extent that fluctuations in the latter allow such a comparison.

The paper is organized as follows. Section 2 outlines the computational strategy employed in somewhat greater detail than described above. Section 3 reviews the details of the molecular model adopted and the MD algorithm employed to conduct the transient relaxation simulations. Section 4 presents the Rouse model equations describing the evolution in time of the quantities which are monitored during the transient MD simulations. Results from detailed atomistic simulations on two systems studied, a C_{24} and a C_{78} PE melt, are presented in section 5. In section 5 we also discuss how the simulation results compare against the predictions of the Rouse model and against previous results obtained from MD simulations on the same systems under equilibrium conditions. Section 6 summarizes the main conclusions of the present work.

2. Computational Strategy

Our computational strategy for simulating stress relaxation upon cessation of steady-state uniaxial elongational flow involves three stages.

Stage I: Generation of Oriented Configurations. In the first stage, termed stage I, a coarse-grained description of the polymer melt is invoked through the definition of the conformation tensor, $\tilde{\mathbf{c}}$, which is an overall, global descriptor of the long length-scale conformation of polymer chains. $\tilde{\mathbf{c}}$ is defined as the second moment tensor of the end-to-end distance vector of a polymer chain reduced by one-third the unperturbed end-to-end distance and averaged over all chains in the system:

$$\tilde{\mathbf{c}}(t) = 3\left\langle \frac{\mathbf{R}(t)\mathbf{R}(t)}{\langle R^2 \rangle_o} \right\rangle \tag{1}$$

In the above equation **R** stands for the end-to-end vector of a macromolecule and $\langle R^2 \rangle_0$ is the mean-squared magnitude of that vector in the equilibrium, quiescent state, where chains are unperturbed to an excellent approximation.[24,25]

The Helmholtz free energy per chain A/N_{ch} is assumed to be a function not only of the mass density ρ and temperature T of the melt but also of the conformation tensor $\tilde{c}$ (eq 20 in ref 24). The partial derivatives of the Helmholtz free energy A/N_{ch} with respect to ρ and $\tilde{c}$ define two thermodynamic fields: a scalar pressure-like quantity b and a tensorial thermodynamic field α. The tensorial field α plays the role of a steady-state flow field, whose application can orient and/or deform the chains, depending on its form and the strength of its matrix elements. The case that has interested us mostly in our studies is one wherein the field α has only one nonzero element, the component α_{xx}. The physical meaning of such a form for the field α has been explained in detail in the relevant publications, refs 24 and 28: It corresponds to the case of a steady-state uniaxial elongational flow, with α_{xx} being indicative of the Deborah number of the flow. As such, the quantity α_{xx} can be considered as a product of the longest relaxation time of the polymer melt times the elongational strain rate of the applied steady-state flow field. The higher the value of α_{xx} relative to unity, the more nonlinear the character of the applied elongational flow.

With the above definitions, a series of detailed atomistic EBMC simulations can be initiated on model melt systems at various values of the orienting thermodynamic field α_{xx}, starting from the zero value ($\alpha_{xx} = 0$, equilibrium, quiescent, field-free state). Large ensembles of uniaxially stretched, anisotropic melt configurations can thus be accumulated at prescribed conditions of temperature T, field b, set of relative chemical potentials μ^* defining the distribution of chain lengths, and field strength α_{xx}. The use of the EBMC algorithm ensures full equilibration of the strained configurations at all length scales in all simulations, subject to the imposed α_{xx}. The method has already been applied[24,28] with considerable success to generate oriented and/or deformed PE melt configurations for three different systems, C_{24}, C_{78}, and C_{156} (subscript indicates mean chain length), all characterized by uniform chain length distributions with polydispersity index less than 1.09 (chain length ranging from half the mean to 1.5 the mean chain length); thousands of uncorrelated, strained configurations representative of these melts under conditions of steady-state, uniaxial elongational flow at a variety of α_{xx} values ranging from 0 to 0.75 have been sampled.

Stage II: From Field-on EBMC Simulations to Field-off MD Simulations. In the second stage of the calculations reported in this paper, termed stage II, the field α_{xx}, which causes orientation and/or deformation of the model polymer systems, is removed. The system is thus left to return back to the field-free, equilibrium state, which should be characterized by the absence of any spatial anisotropy. However, the way the system is allowed to return to equilibrium is not unique; the path to be followed depends on the macroscopic boundary conditions imposed on the sample. These define a corresponding statistical ensemble in which the MD simulations tracking the relaxation process must be conducted.

In this work, the MD simulation takes place in the $NTL_x\sigma_{yy}\sigma_{zz}$ statistical ensemble, similar to the ensemble introduced by Ryckaert and Klein[26] for MD simulations of crystalline phases consisting of infinitely long PE chains. The present paper follows the extended $NTL_x\sigma_{yy}\sigma_{zz}$ ensemble formalism by Yang et al.,[7–8] for studying the dynamics of glassy polymer systems in uniaxial deformation. In this ensemble, the variables kept constant are: the total number of chains N_{ch} and the length of each chain, therefore the total number of interacting mers N; the temperature T; the length L_x of the simulation box in the direction of elongation x; and the average normal stress $(\sigma_{yy} + \sigma_{zz})/2$ in the lateral directions y and z, set equal to minus the ambient atmospheric pressure P_{ext} (i.e., $[\sigma_{yy}(t) + \sigma_{zz}(t)]/2 = -P_{ext}, \forall\ t > 0$). These are the macroscopic constraints encountered following the process of fiber spinning at the end of the spinning operation, when the fibers are kept at constant extension and the stress σ_{xx} in the direction of pulling is allowed to relax from its initial value to the equilibrium, field-free value, equal to $-P_{ext}$ (i.e., $\sigma_{xx}(t \to \infty) = -P_{ext}$). On the other hand, the length of the simulation box in the directions y and z is free to change, so that the instantaneous volume of the system is consistent with the instantaneous value of the stress component σ_{xx}. (Of course, at the end of the simulation, when the system has fully returned to equilibrium, the volume ought to be equal to the one corresponding to the density of the equilibrium system.)

In addition to monitoring the temporal evolution of the stress component $\sigma_{xx}(=\sigma_{xx}(t))$ during the $NTL_x\sigma_{yy}\sigma_{zz}$ MD simulations, we also observe and record as a function of time t the evolution of certain ensemble-averaged descriptors of the chain long length-scale configuration. These descriptors include the diagonal components of the chain conformation tensor ($\tilde{c}_{xx}$, $\tilde{c}_{yy}$, and $\tilde{c}_{zz}$) and the chain mean-square end-to-end distance $\langle R^2 \rangle$. The time evolution of all these quantities contains important information about the system, since it can ultimately be related to the spectrum of relaxation times characterizing the dynamics of the normal modes of the system.[27] The simulation results for the evolution of these quantities are fit to closed-form equations arising from analyzing the dynamics of the system through a coarse-grained molecular model. This is undertaken in the third stage of the methodology.

Stage III: Mapping to a Coarse-Grained Model of Dynamics. In the third stage, termed stage III, first a well-established coarse-grained theoretical model of polymer dynamics is chosen and then equations are derived based on the coarse-grained model, which express the evolution of the system structure and of the stress tensor in the rheological experiment considered. The ensemble averaged results from the MD simulations are mapped onto these equations to extract the coarse-grained model parameters, and therefore the material functions of interest, from chemical constitution. For unentangled polymers, an appropriate coarse-grained molecular model is the Rouse model.[21] This model is widely recognized to offer a reliable estimation of the dynamic properties of many polymer melts (linear, star, branched, etc.) as long as the melt molecular weight (MW) is below the characteristic MW for the formation of entanglements.[27] Dynamics in the Rouse model is best described in terms of the normal coordinates or normal modes. These are certain linear combinations of the atomic positions, each being capable of

independent motion governed by its own characteristic time. The set of characteristic times for all normal modes in the system is called *the spectrum of relaxation times*. According to the Rouse model, knowledge of the spectrum of relaxation times and of the equilibrium density and mean-square unperturbed chain end-to-end distance, $\langle R^2 \rangle_0$, is sufficient for calculating all linear viscoelastic properties of the melt, such as the zero-shear-rate viscosity, η_0, and the shear stress relaxation modulus, $G(t)$.

Our computational strategy is based upon the following testable assumptions: (i) The starting configurations, obtained through EBMC in the presence of an orienting field, are representative of those expected for the actual polymer system having obtained steady state at constant applied elongational strain rate. Strong support for this assumption is provided by comparison of properties of the oriented configurations sampled by EBMC against experiment. For example, the index of refraction and stress tensors calculated from the oriented configurations conform to the stress optical law, with a stress optical coefficient in excellent agreement with that measured in polyethylene melts.[28] (ii) The degree of prealignment introduced in the initial configurations corresponds to an effective strain rate that is low enough for the subsequent relaxation experiment to lie entirely within the linear response regime. This is ensured by the use of α_{xx} values which are always lower than 0.75 in sampling the initial configurations. The physical interpretation of α_{xx} as a strain rate multiplied by the longest relaxation time, i.e., as a Deborah number, is supported by our previous studies of the free energy and stress in such oriented melts.[24] Furthermore, the practical coincidence of the relaxation time spectrum extracted from the current nonequilibrium simulations to that extracted earlier from equilibrium MD simulations of the same systems[20] demonstrates a posteriori that our computer experiments have been conducted in the linear regime. (iii) At any point along the relaxation experiment, the stress tensor can be computed from the conformation tensor $\tilde{\mathbf{c}}$ and the fields b and α through our free-energy based expression, eq 8 of ref 24. This expression has been tested under steady-state flow conditions in refs 24 and 28. It is further tested under transient conditions in this work, by direct comparison against stress values calculated by the molecular virial theorem and found to be fully consistent with the latter. Use of this thermodynamic expression affords calculating the stress with much less statistical noise than would otherwise be possible.

3. Molecular Model and Details of the MD Algorithm

The molecular model used in the present study is exactly the same as in our previous work on the equilibrium dynamic properties of polydisperse, linear PE melts.[20] The model makes use of the united-atom description for methylene and methyl groups, each one of which is considered as a single Lennard–Jones interaction site. Nonbonded interactions are described by a Lennard–Jones potential of the form

$$V_{LJ}(r) = 4\epsilon\left[\left(\frac{\sigma}{r}\right)^{12} - \left(\frac{\sigma}{r}\right)^6\right] \quad (2)$$

with $\epsilon = 0.098$ kcal/mol and $\sigma = 3.94$ Å. $V_{LJ}(r)$ describes all intermolecular site–site interactions as well as

intramolecular interactions between sites separated by more than three (and not four, as mentioned by oversight in ref 20) bonds. A potential cutoff distance of 9.062 Å is used. Attractive tail contributions were dealt with through direct integration.[30] A bond-bending potential of the form[29]

$$V_{bending}(\theta) = \frac{1}{2}K_\theta(\theta - \theta_0)^2 \quad (3)$$

is also used for every skeletal bond angle θ, with $K_\theta = 115.2$ kcal/mol rad^{-2} and $\theta_0 = 112°$. Associated with each dihedral angle ϕ is a torsional potential of the form[31]

$$V_{torsional}(\phi) = c_0 + c_1 \cos\phi + c_2 (\cos\phi)^2 + c_3 (\cos\phi)^3 + c_4 (\cos\phi)^4 + c_5 (\cos\phi)^5 \quad (4)$$

with $c_0 = 2.217$, $c_1 = 2.905$, $c_2 = -3.135$, $c_3 = -0.731$, $c_4 = 6.271$, and $c_5 = -7.527$ in kcal/mol.

Adjacent methyl and methylene groups are maintained at a fixed distance $l = 1.54$ Å apart. Constraint forces associated with fixed bond length constraints are determined using the method of Edberg, Evans, and Moriss.[32] A Fixman potential[33] is also introduced in the MD simulation to make the model sample the configuration-space probability density characteristic of a flexible model in the limit of infinitely stiff bond stretching force constants.[34] A complete discussion on the form of the Fixman potential and how it is calculated during the MD simulations has been presented in our previous work.[20]

As already explained in the previous section, all results reported in this work have been obtained from MD simulations carried out in the statistical ensemble $NTL_x\sigma_{yy}\sigma_{zz}$. This ensemble can be viewed as a hybrid between the well-known NVT ensemble in the x direction and the isothermal−isobaric (NPT) ensemble in the y and z directions. The temperature T is kept fixed at a prescribed value, by employing the Nosé −Hoover thermostat;[35,36] the latter introduces an additional dynamical variable in the system, the parameter s, for which an evolution equation is derived. Also kept constant during the simulation is the box length L_x in the x direction; on the contrary, the box lengths in the other two directions, L_y and L_z, respectively, although always kept equal, are allowed to fluctuate. This is achieved by making use in the simulation of an additional dynamical variable, the cross-sectional area A ($=L_yL_z$) of the simulation cell in the yz plane, for which a suitable equation of motion is derived involving the instantaneous average normal stress ($\sigma_{yy} + \sigma_{zz}$)/2 in the two lateral directions y and z, respectively. This quantity remains constant on average and is equal to $-P_{ext}$ throughout the simulation.

We have followed the formulation of Yang et al.[7] in deriving our equations of motion. The Lagrangian is written as a function of the "extended" variables $\{\tilde{\mathbf{R}}_\kappa, \mathbf{x}_{i\kappa}, A, s\}$ where $\tilde{\mathbf{R}}_\kappa$ is the scaled (with respect to the box edge lengths) position of the center of mass of every chain κ, and $\mathbf{x}_{i\kappa}$ is the position of atom i in chain κ measured relative to the chain center of mass. These variables are "extended" in the sense that they invoke a scaled coordinate system and their time derivatives are always with respect to a "virtual" time t'. The equations of motion derived from the Lagrangian are easily recast in terms of real coordinates and real time.

The total Hamiltonian of the system, derived from the Lagrangian

$$H_{NTL_x\sigma_{yy}\sigma_{zz}} = \sum_i \frac{p_i^2}{2m_i} + V(\mathbf{r}) -$$
$$\frac{1}{2}\sum_\kappa\sum_i \lambda_i^\kappa \left((\mathbf{r}_{i+1,\alpha} - \mathbf{r}_{i,\alpha})^2 - l^2\right) + \frac{Q}{2}\left(\frac{\dot{s}}{s}\right)^2 +$$
$$(g+1)\frac{\ln s}{\beta} + \frac{W}{2}\left(\frac{\dot{A}}{s}\right)^2 + P_{ext}L_x A \quad (5)$$

should be conserved during the run. The first term on the right-hand side represents the kinetic energy, the second term is the potential energy (including the Fixman potential), the third term is the contribution to the Hamiltonian due to constraint bond lengths with λ_i^κ being the Lagrange multiplier for the ith bond of chain κ,[32] and the last four terms are the contributions due to the thermostat and the fluctuating box cross-sectional area in the plane yz. In our MD runs, $H_{NTL_x\sigma_{yy}\sigma_{zz}}$ was found to change by less than 1% within 1 ns of simulation.

4. Calculations by the Rouse Model and Averaging over MD Trajectories

As already stated in section 2, stage III of our methodology involves mapping atomistic simulation results for the temporal evolution of certain averaged quantities onto a coarse-grained theoretical model, the aim being to extract the spectrum of relaxation times of the system. For unentangled polymers, such as the C_{24} and C_{78} PE melts studied in the previous[20] and present work, the Rouse model is a suitable coarse-grained molecular model. In ref 20, we presented the basic assumptions of the Rouse model and reviewed its formulation in terms of the normal modes. Particular emphasis was placed on the equations describing the relaxation of the normal modes and the mean-square displacement of the chain center of mass under equilibrium conditions. We showed that, by suitably mapping the simulation results onto the Rouse model equations, one can extract (a) the spectrum of relaxation times, τ_p, $p = 1, 2, ..., N$ and (b) the friction factor ζ quantifying the frictional force felt by a monomer in the melt as it moves through the environment formed by all other mers.

In the present work we will extend the analysis to a system which, initially, is away from equilibrium, and which, subsequently, is allowed to return to equilibrium by releasing the macroscopic field that keeps it in a steady-state nonequilibrium state. More specifically, we will be concerned with a melt of linear chains that have been oriented by means of a steady-state elongational flow field, represented in our simulations by the imposed tensorial thermodynamic field α_{xx}. Initially the melt is in a steady state away from equilibrium, with all microscopic elements of its structure fully adjusted to the imposed α_{xx}.[24,28] At time $t = 0$ the field α_{xx} is switched off and the system is allowed to return to equilibrium, keeping the length L_x constant and the average lateral normal stress $(\sigma_{yy} + \sigma_{zz})/2$ equal to $-P_{ext}$.

The purpose of the present section is to use the Rouse model in order to derive the equations describing the time evolution of the stress tensor component σ_{xx} and of the conformation tensor component $\tilde{c}_{xx}$ for this stress relaxation experiment.

4.1. Relaxation of the Stress Component σ_{xx}. The starting point for the calculation of the stress tensor component σ_{xx} according to the Rouse model is eq 4.137 in section 4.5.2 of ref 27:

$$\sigma_{xx}(t) = \frac{N_{ch}}{V}\sum_{p=1}^N k_p\langle X_{px}(t)X_{px}(t)\rangle \quad (6)$$

with X_p being the mode of order p and k_p the spring constant corresponding to the pth mode

$$k_p = \frac{6\pi^2 k_B T}{\langle R^2\rangle_0}p^2, \quad p = 1, 2, ..., N \quad (7)$$

According to eq 6, to calculate σ_{xx} we need to calculate the average quantity $\langle X_{px}(t)X_{px}(t)\rangle$ over all stochastic trajectories consistent with the correct initial and boundary conditions. To do this, we will use the Smoluchowski equation. During the process of relaxation ($t > 0$), no external field is exerted on the chains; therefore, for times $t > 0$, the form of the Smoluchowski equation, eq 4.141 in section 4.5.3 of 27, that should be considered is the one corresponding to a velocity gradient field $\kappa_{\alpha\beta} = 0 \; \forall \; \alpha, \beta$:

$$\frac{\partial}{\partial t}\langle X_{px}(t)X_{px}(t)\rangle = -\frac{2p^2}{\tau_R}\left(\langle X_{px}(t)X_{px}(t)\rangle - \frac{k_B T}{k_p}\right) \quad (8)$$

where τ_R (=τ_1) represents the Rouse or longest relaxation time of the chain. The relaxation time τ_p of the higher modes are expressed in terms of τ_R as $\tau_p = \tau_R/p^2$. The friction constants ζ_p for modes $p \geq 1$ satisfy $\zeta_p = k_p\tau_p$.

To solve eq 8, we need to provide an initial condition for the unknown quantity $\langle X_{px}(t)X_{px}(t)\rangle$ for $t = 0$. The time $t = 0$ coincides with the moment the field is just turned off, that is, the value $\langle X_{px}(t = 0)X_{px}(t = 0)\rangle$ is representative of the steady-state elongational flow period that precedes the relaxation under investigation. The value of this quantity is of course a function of the elongational flow field α_{xx}, applied previously in the course of the field-on EBMC simulations.

To calculate $\langle X_{px}(t)X_{px}(t)\rangle$ at the end of the steady-state elongational flow, we will invoke again the Smoluchowski equation. Since the field α_{xx} is exerted on the melt during the entire duration of the steady-state elongational flow, the form of the Smoluchowski equation that should be considered in this case is that corresponding to a velocity gradient field with all other components zero except for the xx component, which equals α_{xx}/τ_R. By applying eqs 7.156−7.159 of ref 27

$$\frac{\partial}{\partial t}\langle X_{px}(t)X_{px}(t)\rangle = 2\frac{k_B T}{\zeta_p} - 2\left(\frac{k_p}{\zeta_p} - \frac{\alpha_{xx}}{\tau_R}\right)\langle X_{px}(t)X_{px}(t)\rangle \quad (9)$$

with initial condition corresponding to an equilibrium undeformed melt:

$$\text{at } t = 0, \quad \langle X_{px}(0)X_{px}(0)\rangle = \frac{k_B T}{k_p} \quad (10)$$

The solution to the initial value problem of eqs 9−10 is given by

$$\langle X_{px}(t)X_{px}(t)\rangle = \frac{k_B T}{k_p}\left(\frac{p^2}{p^2-\alpha_{xx}}\right) - \frac{k_B T}{k_p}\left(\frac{\alpha_{xx}}{p^2-\alpha_{xx}}\right)\exp\left(-2(p^2-\alpha_{xx})\frac{t}{\tau_R}\right) \quad (11)$$

From eq 11 it is seen that the steady-state value of the quantity $\langle X_{px}(t)X_{px}(t)\rangle$ under the applied field value α_{xx} is

$$\lim_{t\to\infty}\langle X_{px}(t)X_{px}(t)\rangle = \frac{1}{1-\dfrac{\alpha_{xx}}{p^2}}\frac{k_B T}{k_p} \equiv B_{xx,p}\frac{k_B T}{k_p} \quad (12)$$

where

$$B_{xx,p} = \frac{1}{1-\dfrac{\alpha_{xx}}{p^2}}$$

denotes the factor by which the variance of the pth mode $\langle X_{px}(t)X_{px}(t)\rangle$ increases at steady-state under the applied field value α_{xx} relative to equilibrium. Clearly, $B_{xx,p} > 1$. In addition, eq 12 shows that the higher the value of p the smaller the relative increase of the corresponding averaged quantity $\langle X_{px}(t)X_{px}(t)\rangle$.

The value of the averaged quantity $\langle X_{px}(t)X_{px}(t)\rangle$ at $t = \infty$ for the steady-state elongational flow is the initial condition that should be used in conjunction with eq 8 in order to calculate the temporal evolution of the quantity $\langle X_{px}(t)X_{px}(t)\rangle$ during the field-off relaxation process. The result is

$$\langle X_{px}(t)X_{px}(t)\rangle = \frac{k_B T}{k_p}\left(1 + (B_{xx,p}-1)\exp\left(-\frac{2t}{\tau_p}\right)\right) \quad (13)$$

By substituting eq 13 into eq 6 and rearranging terms, we end up with the following equation describing the stress relaxation during the $NTL_x\sigma_{yy}\sigma_{zz}$ experiment:

$$\frac{\sigma_{xx}(t)-\sigma_{xx}(\infty)}{\sigma_{xx}(0)-\sigma_{xx}(\infty)} = \frac{\sum_{p:\text{all}}(B_{xx,p}-1)\exp\left(-\dfrac{2t}{\tau_p}\right)}{\sum_{p:\text{all}}(B_{xx,p}-1)} \quad (14)$$

Here $\sum_{p:\text{all}}(\equiv\sum_{p=1}^{\infty})$ denotes summation over all positive integer numbers p. $\sigma_{xx}(0)$ is the value of $\sigma_{xx}(t)$ at time $t = 0$; in our atomistic simulations this corresponds to the end of the EBMC simulations or equivalently to the beginning of the $NTL_x\sigma_{yy}\sigma_{zz}$ MD simulations. Similarly, $\sigma_{xx}(\infty)$ is the value of $\sigma_{xx}(t)$ at time $t = \infty$; clearly, $\sigma_{xx}(\infty) = -P_{\text{ext}}$.

Equation 14 is the equation describing the relaxation of the stress component $\sigma_{xx} = \sigma_{xx}(t)$ in the computational experiments carried out in the present work, according to the Rouse model. It is this equation against which the $NTL_x\sigma_{yy}\sigma_{zz}$ MD simulations results ought to be compared in order to extract the spectrum of relaxation times τ_p, $p = 1, 2, ...,$ of the system.

4.2. The Relaxation of the Conformation Tensor Component $\tilde{c}_{xx}$. In terms of the normal coordinates, $\tilde{c}_{xx}$, defined through eq 1, is given by the following equation:[27]

$$\tilde{c}_{xx}(t) = \frac{3}{\langle R^2\rangle_0}16\sum_{p:\text{odd}}\langle X_{px}(t)X_{px}(t)\rangle \quad (15)$$

Thus, by directly substituting eq 13 for $\langle X_{px}(t)X_{px}(t)\rangle$ into eq 15, and after rearranging terms, we obtain

$$\frac{\tilde{c}_{xx}(t)-\tilde{c}_{xx}(\infty)}{\tilde{c}_{xx}(0)-\tilde{c}_{xx}(\infty)} = \frac{\sum_{p:\text{odd}}\dfrac{(B_{xx,p}-1)}{k_p}\exp\left(-\dfrac{2t}{\tau_p}\right)}{\sum_{p:\text{odd}}\dfrac{(B_{xx,p}-1)}{k_p}} \quad (16)$$

As with the relaxation of the stress component σ_{xx}, $\tilde{c}_{xx}(0)$ is the value of $\tilde{c}_{xx}(t)$ at time $t = 0$, i.e., at the end of the EBMC simulations or equivalently at the beginning of the $NTL_x\sigma_{yy}\sigma_{zz}$ MD simulations. Similarly, $\tilde{c}_{xx}(\infty)$ is the value of $\tilde{c}_{xx}(t)$ at time $t = \infty$ of the stress relaxation experiment; clearly, $\tilde{c}_{xx}(\infty) = 1$.

Equation 16 is the pertinent equation describing the relaxation of the conformation tensor component $\tilde{c}_{xx} = \tilde{c}_{xx}(t)$ in the computational experiments of the present work, according to the Rouse model. As with eq 14 for the stress tensor component σ_{xx}, eq 16 offers an additional way for extracting the spectrum of relaxation times τ_p, $p = 1, 2, ...,$ by fitting the simulation results for the relaxation of the quantity $\tilde{c}_{xx}$.

An important point to notice about eqs 14 and 16 is that the longest time governing the relaxation of the stress and conformation tensor components, $\sigma_{xx}(t)$ and $\tilde{c}_{xx}(t)$, is $\tau_R/2$. This is half the time characterizing the decay of the time autocorrelation function of the first normal mode ($p = 1$) in the equilibrium state

$$\langle \mathbf{X}_p(t)\cdot\mathbf{X}_p(0)\rangle = \frac{k_B T}{k_p}\exp\left(-\frac{t}{\tau_p}\right) = \frac{Nb^2}{6\pi^2}\frac{1}{p^2}\exp\left(-\frac{t}{\tau_p}\right) \quad (17)$$

and half the longest relaxation time governing the decay of the autocorrelation function of the end-to-end vector at equilibrium

$$\frac{\langle \mathbf{R}(t)\cdot\mathbf{R}(0)\rangle}{\langle R^2\rangle_0} = \sum_{p=\text{odd}}\frac{8}{p^2\pi^2}\exp\left(-\frac{tp^2}{\tau_1}\right) \quad (18)$$

In the case of the oriented configurations the autocorrelation function of the end-to-end vector $\langle \mathbf{R}(t)\cdot\mathbf{R}(0)\rangle$ can also be calculated. This function can be obtained as[27]

$$\langle \mathbf{R}(t)\cdot\mathbf{R}(0)\rangle = 16\sum_{p:\text{odd}}\langle \mathbf{X}_p(t)\cdot\mathbf{X}_p(0)\rangle \quad (19)$$

To calculate the quantities $\langle \mathbf{X}_p(t)\cdot\mathbf{X}_p(0)\rangle$ we follow the same procedure as we did for $\langle \mathbf{X}_p(t)\cdot\mathbf{X}_p(t)\rangle$ in the case of conformation and stress tensors. During the process of relaxation the quantity $\langle \mathbf{X}_p(t)\cdot\mathbf{X}_p(0)\rangle$ follows the Smoluchowski equation

$$\frac{\partial}{\partial t}\langle X_{p\gamma}(t)X_{p\epsilon}(0)\rangle = -\frac{p^2}{\tau_R}\langle X_{p\gamma}(t)X_{p\epsilon}(0)\rangle, \quad \forall, \gamma, \epsilon \quad (20)$$

with the same boundary condition, eq 12, introduced above

$$\langle X_{p\gamma}(t)X_{p\epsilon}(0)\rangle = B_{\gamma\epsilon,p}\frac{k_B T}{k_p} \quad (21)$$

and

$$B_{\gamma\epsilon,p} = \begin{cases} \dfrac{1}{1 - \dfrac{\alpha_{xx}}{p^2}} & \text{if } \gamma = \epsilon = x, \\ 1, & \text{otherwise} \end{cases} \quad (22)$$

By solving the above equation, we can obtain $\langle \dot{X}_{p\gamma}(t)X_{p\epsilon}(0)\rangle$:

$$\langle X_{p\gamma}(t)X_{p\epsilon}(0)\rangle = B_{\gamma\epsilon,p}\frac{k_B T}{k_p}\exp\left(-\frac{t}{\tau_p}\right) \quad (23)$$

Finally, by substituting in eq 19 the autocorrelation functions of the modes, we get

$$\frac{\langle \mathbf{R}(t)\cdot\mathbf{R}(0)\rangle}{\langle R^2\rangle_0} =$$

$$\sum_{p=\text{odd}}\left[\frac{8}{3p^2\pi^2}\left(2 + \frac{1}{1 - \dfrac{\alpha_{xx}}{p^2}}\right)\exp\left(-\frac{tp^2}{\tau_1}\right)\right] \quad (24)$$

As we can see, the dominant characteristic time for the decay of the end-to-end vector under the nonequilibrium relaxation conditions considered is again τ_R, exactly as under equilibrium conditions (eq 18).

The quantities $\tilde{c}_{xx}$ and σ_{xx} decay with characteristic time $\tau_R/2$ and not τ_R because they are related to the *second moment* of **R**. This means that, by observing the relaxation of the stress or conformation tensor of the prestrained system back to equilibrium, one can extract the spectrum of relaxation times τ_p, $p = 1, 2, ...,$ in half the CPU time that would be required for monitoring the decay of the time autocorrelation function of the normal modes of the same system at equilibrium, or the decay of the autocorrelation function of the end-to-end vector under equilibrium or nonequilibrium conditions. This is a significant observation, since it reduces by a factor of 2 the problem of long relaxation times which plagues dynamic simulations of long-chain systems. This advantage, however, occurs at a price, namely a larger statistical error in the dynamical information that can be accumulated within a single MD run. During the transient relaxation of the prestrained system, the system state evolves continuously, thus rendering impossible the application of the usual equilibrium MD trick of multiple time origins for reducing the statistical uncertainty of computed time correlation functions. The advantage of time translation invariance of equilibrium simulations is lost. In the relaxation experiments considered here, the only way to reduce the large fluctuations present in $\sigma_{xx}(t)$ and $\tilde{c}_{xx}(t)$ is to average over many MD runs initiated at different strained configurations, all runs conforming to the same macroscopic $NTL_x\sigma_{yy}\sigma_{zz}$ conditions. This means that *a large number* of initially prestrained configurations need to be subjected to $NTL_x\sigma_{yy}\sigma_{zz}$ MD simulations; the ensemble-averaged results at every time instant t will be those corresponding to averages at time t over all nonequilibrium trajectories generated in this way. As will be seen immediately below, such averaging over many dynamical trajectories quickly reduces the statistical uncertainty of structural results and leads to rather smooth

curves. Usually, averaging over about 100 trajectories is found to be sufficient for the results at every time instant to be calculated with an error less than about only a few percent. Ideally, for the particular system studied and the particular α_{xx} value with which the system has been brought to the oriented state, *all* strained configurations sampled during the EBMC run could be used in the averaging process. One should note that each set of MD simulations starting from different configurations corresponding to the same α_{xx} can be conducted in parallel, thus greatly reducing the time required for obtaining the rheological properties.

4.3. Calculation of the Stress by MD. In the simulations, the stress tensor is calculated in two ways: the first is by applying the molecular virial theorem.[37] The use of the molecular stress tensor relies on scaling molecular center-of-mass positions with the boundaries of the simulation box, while holding all intramolecular distances constant. For model systems consisting of macromolecules of overall dimensions comparable to the simulation box size, this scaling of space is quite inhomogeneous. This has not been observed to cause problems in simulation practice. Trial calculations based on the atomic stress tensor, with due consideration of the constraint forces on the interaction sites, have led to results indistinguishable from those obtained by the molecular virial theorem. It is noted that localizing the momentum on center of mass positions or on atomic positions for the purpose of calculating the stress are just two of an infinite number of possibilities,[38] all of which give the same average stress tensor under equilibrium or steady-state conditions. The time autocorrelation function of the instantaneous stress at short times may depend on which definition is used for the stress. However, the integral underneath it is invariant and is related to the viscosity (see below).

The second way implemented in this work to calculate the stress is to use the Helmholtz energy function and affine deformation assumption extensively discussed in refs 24 and 28. According to the latter approach, the stress tensor at every time t can be calculated from the ensemble-averaged values of mass density ρ, conformation tensor $\tilde{c}_{xx}$ and partial derivative of the Helmholtz energy function with respect to $\tilde{c}_{xx}$ at time t, through

$$\sigma_{xx}(t) =$$
$$-P_{\text{ext}} + 2\frac{R}{M}T\rho(t)\tilde{c}_{xx}(t)\left[\frac{\partial(A/N_{\text{ch}})}{\partial\tilde{c}_{xx}}\bigg|_{T,\rho,\tilde{c}_{[xx]}}\right]_{\tilde{c}_{xx}=\tilde{c}_{xx}(t)} \quad (25)$$

where P_{ext} denotes the equilibrium (atmospheric) pressure and M the number-average molecular weight of the system. In writing down eq 25, the assumption has been made that, due to the elongational character of the stress relaxation process, the ensemble-averaged values of all off-diagonal components of the conformation tensor are identically zero; this assumption is confirmed by our MD simulations. In eq 25, the symbolism $[\partial(A/N_{\text{ch}})/\partial\tilde{c}_{xx}|_{T,\rho,\tilde{c}_{[xx]}}]_{\tilde{c}_{xx}=\tilde{c}_{xx}(t)}$ denotes the partial derivative of the Helmholtz energy per chain with respect to $\tilde{c}_{xx}$ at a value of $\tilde{c}_{xx}$ equal to that characterizing the melt at time t. The latter value of $\tilde{c}_{xx}$ is calculated as an ensemble average at time t over all MD trajectories initiated at configurations corresponding to the same steady-state elongational flow state. The function $\partial(A/N_{\text{ch}})/\partial\tilde{c}_{xx}|_{T,\rho,\tilde{c}_{[xx]}}$ $(=\alpha_{xx})$ has been accumulated and plotted against $\tilde{c}_{xx}$ in our elasticity calculations.[24] Here it is
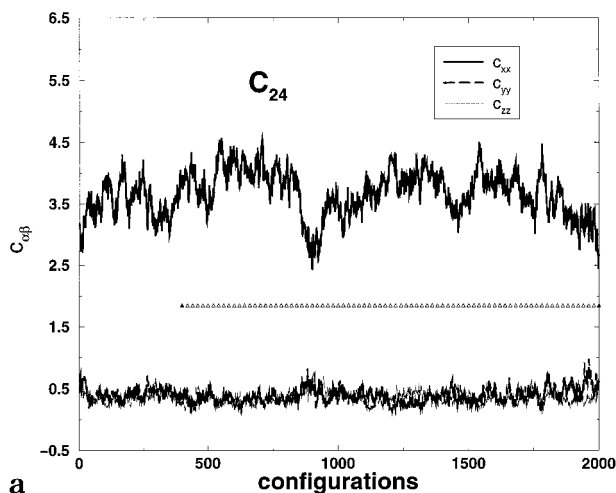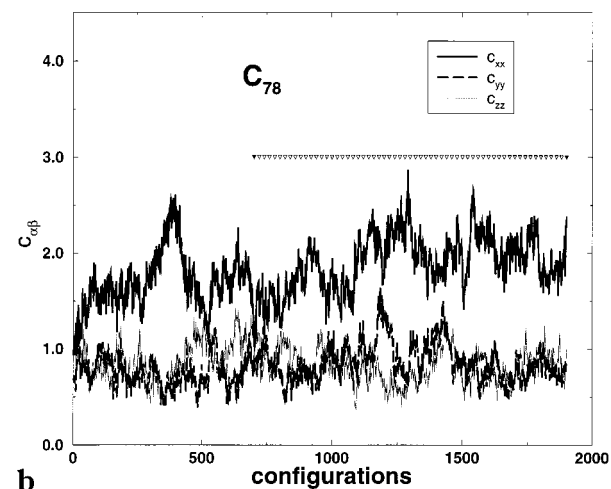
Figure 1. Schematic showing the plateau region from which prestrained configurations, obtained by using the EBMC algorithm in the presence of the orienting field α_{xx}, were chosen to be subjected to $NTL_x\sigma_{yy}\sigma_{zz}$ MD simulations, for (a) the C_{24} and (b) the C_{78} PE melt systems. Because of CPU time limitations, only a small representative sample of these configurations was chosen for the $NTL_x\sigma_{yy}\sigma_{zz}$ MD simulations. The actual configurations used are indicated by the open triangles and the two filled triangles on each end.

obtained by looking up the value of α_{xx} corresponding to $\tilde{c}_{xx}$ in the $\tilde{c}_{xx}(\alpha_{xx})$ plots of Figure 7 of ref 24.

5. Results

Results will be presented from averaging over about 100 $NTL_x\sigma_{yy}\sigma_{zz}$ MD trajectories for each stress relaxation experiment, initiated at ensembles of strained configurations of two PE melt systems: a 32-chain C_{24} and a 40-chain C_{78} PE melt. The reader is reminded that each melt is labeled by its number-average chain length $\bar{X}$; both melts are characterized by uniform chain length distributions, ranging from $\bar{X}/2$ to $3\bar{X}/2$. Averages of conformational properties reported here are taken over all chains present in each melt. Extensive end-bridging Monte Carlo (EBMC) simulations have been performed on both model systems in the course of our previous work,[24,28] at various field values α_{xx}. Parts a and b of Figure 1, which have resulted from such EBMC simulations, show the evolution of the conformation tensor components $\tilde{c}_{xx}$, $\tilde{c}_{yy}$, and $\tilde{c}_{zz}$ with CPU time for the two PE melt systems, C_{24} and C_{78}, at field values $\alpha_{xx} = 0.75$ and $\alpha_{xx} = 0.3$, respectively. In Figure 1b one can see
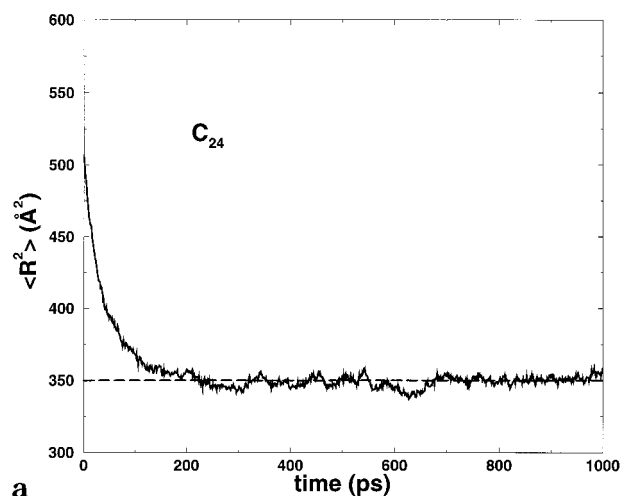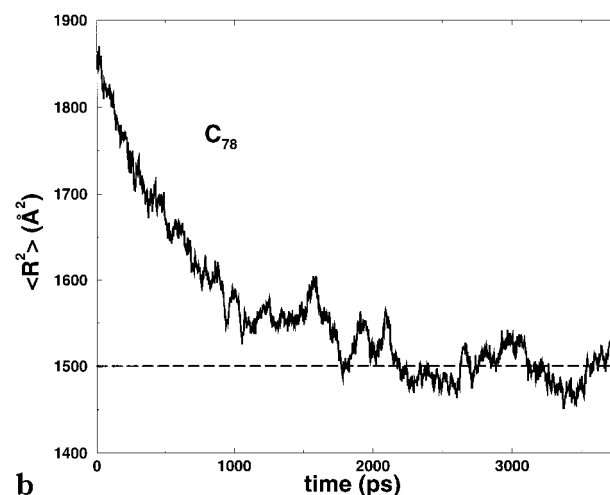
Figure 2. Time evolution of the mean-square chain end-to-end distance $\langle R^2 \rangle$ for (a) the C_{24} and (b) the C_{78} PE melt systems, averaged over all $NTL_x\sigma_{yy}\sigma_{zz}$ trajectories ($T = 450$ K, $P_{ext} = 1$ atm). The dashed lines in the figures show the equilibrium values of the mean square chain end-to-end distance $\langle R^2 \rangle_o$ for the two systems, obtained by EBMC or NVT MD equilibrium simulations.

the transition from the field-free, equilibrium isotropic structure to a structure significantly oriented along the x direction due to the imposed field α_{xx}. In principle, all configurations in the plateau regime of the EBMC simulations (between the filled triangles in Figure 1a,b) are excellent starting points for performing the $NTL_x\sigma_{yy}\sigma_{zz}$ MD simulations. Because of CPU time limitations, however, only about 100 of these configurations were chosen for each system to be subjected to an $NTL_x\sigma_{yy}\sigma_{zz}$ MD simulation. The results shown in the next part of this section have been obtained after averaging over runs initiated at this relatively small number of configurations.

5.1. Equilibrium Conformational Properties. To ensure that, in the limit of very long times, where the stress tensor should have attained its equilibrium value, the $NTL_x\sigma_{yy}\sigma_{zz}$ algorithm behaves as the usual NVT algorithm, we first compared the equilibrium characteristics of melts obtained after long $NTL_x\sigma_{yy}\sigma_{zz}$ simulations against the equilibrium characteristics obtained from end-bridging Monte Carlo simulations at a zero field (i.e., for $\alpha_{xx} = 0$) or from equilibrium MD simulations.

Parts a and b of Figure 2 show the evolution in time

Table 1. Equilibrium Results for the Mean-Square Chain End-to-End Distance $\langle R^2 \rangle$, the Mean-Square Chain Radius of Gyration $\langle R_g^2 \rangle$, and the Specific Volume v for the two PE Melt Systems Studied in the Present Work, As Obtained by Using (a) the Present $NTL_x\sigma_{yy}\sigma_{zz}$ MD Algorithm in the Limit of Long Times, (b) the Equilibrium NVT MD (Ref 20), and (c) the EBMC Algorithm in the Absence of Any Field ($\alpha_{xx} = 0$) ($T = 450$ K and $P_{ext} = 1$ atm)

	C$_{24}$			C$_{78}$		
	$NTL_x\sigma_{yy}\sigma_{zz}$	NVT	EBMC	$NTL_x\sigma_{yy}\sigma_{zz}$	NVT	EBMC
$\langle R^2 \rangle$ (Å^2)	350 ± 20	350 ± 20	350 ± 20	1530 ± 50	1510 ± 40	1490 ± 100
$\langle R_g^2 \rangle$ (Å^2)	50 ± 10	50 ± 10	50 ± 10	220 ± 10	225 ± 20	224 ± 10
v (cm^3/g)	1.419 ± 0.08	1.385	1.409 ± 0.05	1.23 ± 0.05	1.26	1.283 ± 0.003

of the mean square end-to-end distance $\langle R^2 \rangle$ for the C$_{24}$ and C$_{78}$ PE melts studied, averaged over all simulated trajectories. For both systems, the initial values of $\langle R^2 \rangle$ are much higher than the equilibrium ones, indicative of significant elongation of the chains along the x direction due to the imposed field α_{xx}. As time goes on, however, $\langle R^2 \rangle$ in both systems is seen to decrease continuously, approaching an asymptotic value characteristic of the system under field-free, equilibrium conditions. For the C$_{24}$ melt this value is seen to be 350 ± 20 Å^2, whereas for the C$_{78}$ melt it is 1530 ± 50 Å^2. The dashed straight lines in the same figures show the corresponding equilibrium $\langle R^2 \rangle$ values for the C$_{24}$ and C$_{78}$ systems, respectively, as obtained from EBMC or NVT MD simulations on the same systems under field-free, equilibrium conditions.[24,20] These results, together with the corresponding results for the mean- square radius of gyration $\langle R_g^2 \rangle$ and the specific volume v of the two melts, are summarized in Table 1. Clearly, the agreement between EBMC, NVT MD, and $NTL_x\sigma_{yy}\sigma_{zz}$ MD-based results for the equilibrium properties of the two melts is excellent. This shows that, in the limit of infinite time ($t \to \infty$), the correct equilibrium properties are recovered by the $NTL_x\sigma_{yy}\sigma_{zz}$ MD method.

Parts a and b of Figure 3 show the time evolution of the lengths L_x and L_y ($=L_z$) of the model box in the x, y, and z dimensions, averaged over all $NTL_x\sigma_{yy}\sigma_{zz}$ runs on the C$_{24}$ and C$_{78}$ PE melts. As required from the macroscopic restrictions imposed in the $NTL_x\sigma_{yy}\sigma_{zz}$ statistical ensemble, the box length L_x along the strain direction remains constant during the simulation. On the other hand, the lengths L_y and L_z in the other two directions fluctuate. The reader is reminded that the results shown in Figure 3 are actually averages over ca. 100 transient MD trajectories; each individual trajectory shows much higher fluctuations in L_y ($=L_z$). Despite the averaging, an oscillatory "ringing" pattern is seen in the evolution of L_y ($=L_z$). This ringing behavior is caused by the fact that the instantaneous box lengths L_y and L_z do not evolve independently but they are constrained to be equal to each other, as only one dynamic variable, the cross-sectional area A, is integrated in time. Recent simulations[39] in the $NT\sigma_{xx}\sigma_{yy}\sigma_{zz}$ statistical ensemble, where all three box lengths L_x, L_y, and L_z are allowed to evolve independently in time by employing the Berendsen method,[40] are seen not to exhibit this "ringing" behavior. For the C$_{24}$ PE melt, whose density in the strained state is significantly higher than in the field-free state (ref. 24), L_y and L_z are seen to be always above the value of L_x, displaying the tendency of the system to return to the density of the equilibrium state. As mentioned above, the ensemble-average values of L_y and L_z at $t \to \infty$ are such that the density of the system is exactly the one corresponding to the same melt under equilibrium conditions.

5.2. Relaxation of the Chain End-to-End Vector. Parts a and b of Figure 4 present the time autocorrelation function of the scaled end-to-end vector reduced
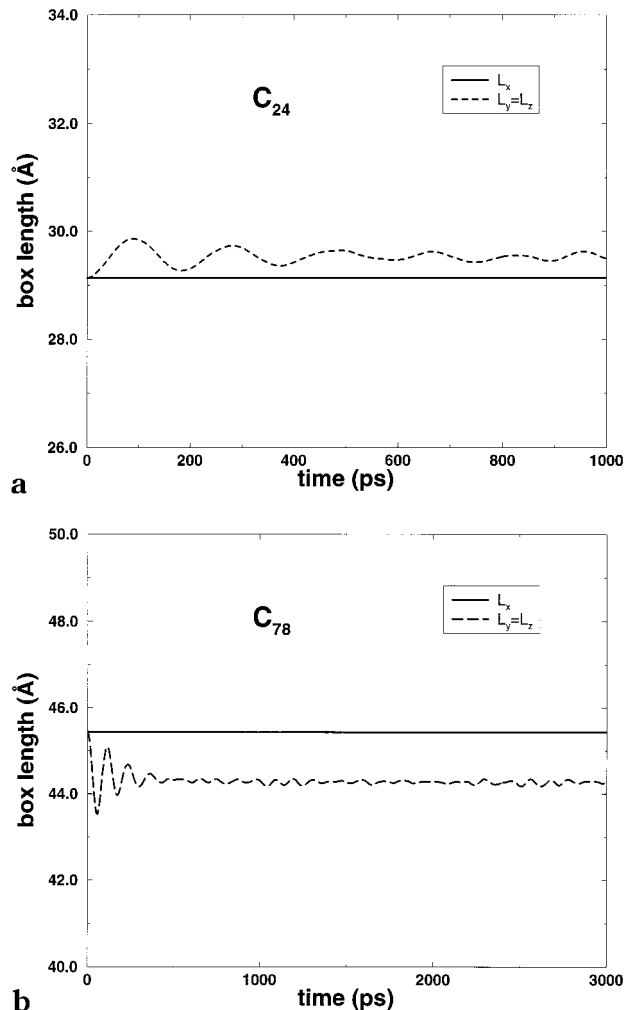

Figure 3. Time evolution of the lengths L_x and $L_y = L_z$ of the simulation box, as obtained from averaging over all simulated trajectories for (a) the C$_{24}$ and (b) the C$_{78}$ PE melt systems ($T = 450$ K, $P_{ext} = 1$ atm).

by the equilibrium mean-square end-to-end distance, $\langle \mathbf{R}(t) \cdot \mathbf{R}(0) \rangle / \langle R^2 \rangle_0$, for the C$_{24}$ and C$_{78}$ PE melt systems, respectively. The rate at which this function approaches zero is a measure of the global relaxation of the chain, because it describes how fast the chain *forgets* its initial configuration. Also shown in the figures (dashed lines) are the corresponding curves obtained from equilibrium NVT simulations on the same systems.[20] The value obtained from the initially strained configurations at time $t = 0$ is larger than 1 because of the orientation in the x direction. The figures show clearly that, for each system, the time scale over which $\langle \mathbf{R}(t) \cdot \mathbf{R}(0) \rangle / \langle R^2 \rangle_0$ drops to zero is the same in both equilibrium and nonequilibrium simulations; it is governed by the Rouse time τ_R. Overall, about 300 ps are needed in the C$_{24}$ melt system and certainly more than 3 ns in the C$_{78}$ melt system for $\langle \mathbf{R}(t) \cdot \mathbf{R}(0) \rangle / \langle R^2 \rangle_0$ to drop to zero. The fact that
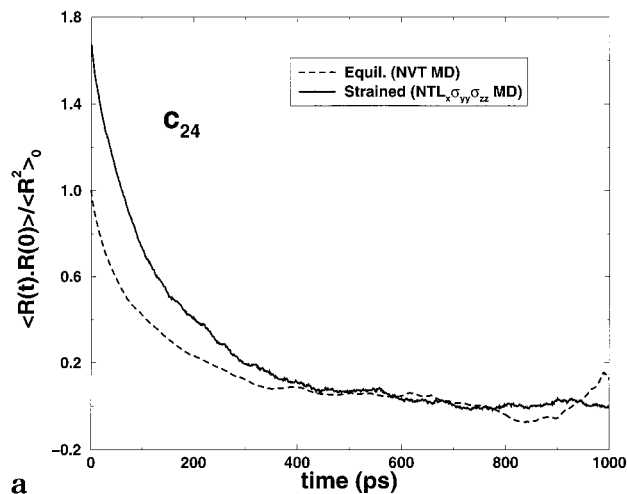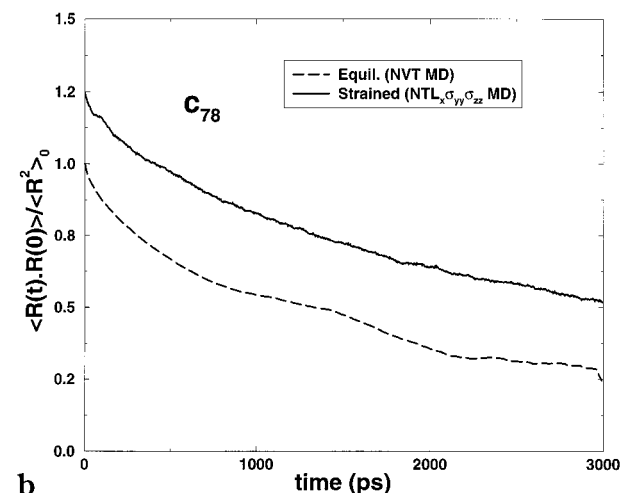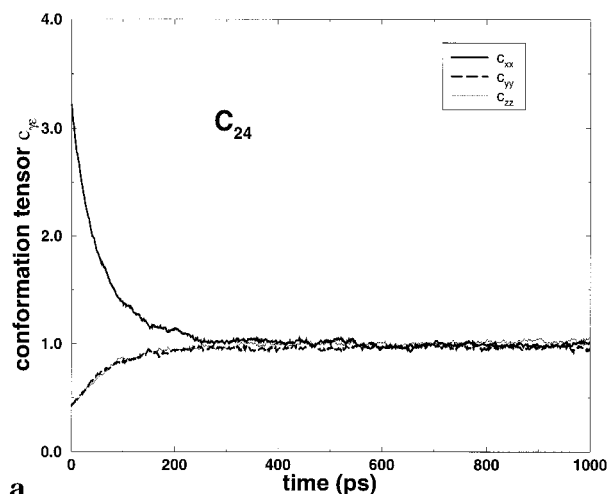
Figure 4. Decay of the scaled chain end-to-end vector orientational autocorrelation function $\langle \mathbf{R}(t) \cdot \mathbf{R}(0) \rangle / \langle R^2 \rangle_0$ in real time t for (a) the C_{24} and (b) the C_{78} PE melt systems. Solid lines correspond to results obtained from the preoriented configurations with the present $NTL_x \sigma_{yy} \sigma_{zz}$ MD algorithm, and dashed lines correspond to results obtained from isotropic configurations with the equilibrium NVT MD algorithm ($T = 450$ K, $P_{ext} = 1$ atm).

Figure 5. Evolution of the diagonal components $\tilde{c}_{xx}$, $\tilde{c}_{yy}$, and $\tilde{c}_{zz}$ of the conformation tensor $\tilde{c}$ with time t for (a) the C_{24} and (b) the C_{78} PE melt systems. Results are averaged over all $NTL_x \sigma_{yy} \sigma_{zz}$ trajectories ($T = 450$ K, $P_{ext} = 1$ atm).

the maximal relaxation time is practically identical under equilibrium and nonequilibrium conditions confirms that the nonequilibrium experiments have been conducted in the linear regime.

5.3. Relaxation of the Conformation Tensor Components. Parts a and b of Figure 5 show the time evolution of the diagonal components, $\tilde{c}_{xx}$, $\tilde{c}_{yy}$, and $\tilde{c}_{zz}$, of the conformation tensor for the C_{24} and C_{78} melt systems, respectively. For both systems the initial value of $\tilde{c}_{xx}$ is significantly higher than 1, whereas those of $\tilde{c}_{yy}$ and $\tilde{c}_{zz}$ are a little smaller than 1, indicative of oriented conformations induced by the imposed steady-state elongational flow field α_{xx}. As time evolves, $\tilde{c}_{xx}$ drops, whereas $\tilde{c}_{yy}$ and $\tilde{c}_{zz}$ increase continuously, approaching the steady-state, field-free value of 1, indicative of fully equilibrated, isotropic structures in the absence of any deforming or orienting field. As already explained in section 4, all these results have been obtained through averaging over about 100 trajectories, all started at configurations oriented by the same value of the steady-state elongational flow field α_{xx}.

An interesting observation about the curves in parts a and b of Figure 5 is the following: Due to the

cylindrical symmetry of the oriented structures, $\tilde{c}_{yy}(t)$ and $\tilde{c}_{zz}(t)$ should be equal at any time t and their time evolutions should be identical. Figure 5a shows this to be indeed true for the C_{24} system. For the C_{78} chain system, however, there appear to be some deviations between $\tilde{c}_{yy}(t)$ and $\tilde{c}_{zz}(t)$. This is a statistical effect resulting from incomplete averaging. This can be understood if we take a look at Figure 1b, which shows the values of the three diagonal components of the conformation tensor in the plateau region of the steady-state elongational flow EBMC simulations. The initial configurations subjected to the $NTL_x \sigma_{yy} \sigma_{zz}$ MD simulations have been taken in their majority from the rightmost part of the plateau region, where $\tilde{c}_{yy}$ is higher than $\tilde{c}_{zz}$. This manifests itself in the deviations seen in the MD relaxation curves. Clearly, a larger number of strained configurations from the plateau region of Figure 1b should be subjected to $NTL_x \sigma_{yy} \sigma_{zz}$ MD simulation in order for the two curves $\tilde{c}_{yy}$ and $\tilde{c}_{zz}$ to fall on top of each other, as happens with the C_{24} system.

5.4. Relaxation of the Stress Tensor Components. Parts a and b of Figure 6 show the time evolution of the stress tensor component σ_{xx} for the C_{24} and C_{78} PE melt systems studied. Two curves are shown in each figure. The thin solid line tracks the evolution of σ_{xx} as obtained from applying the molecular virial theorem on
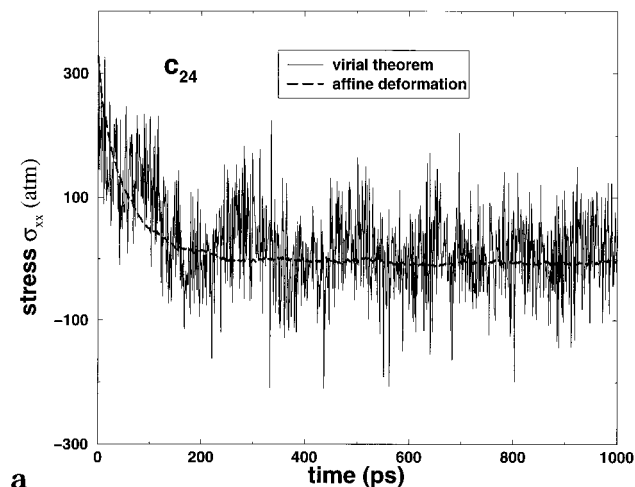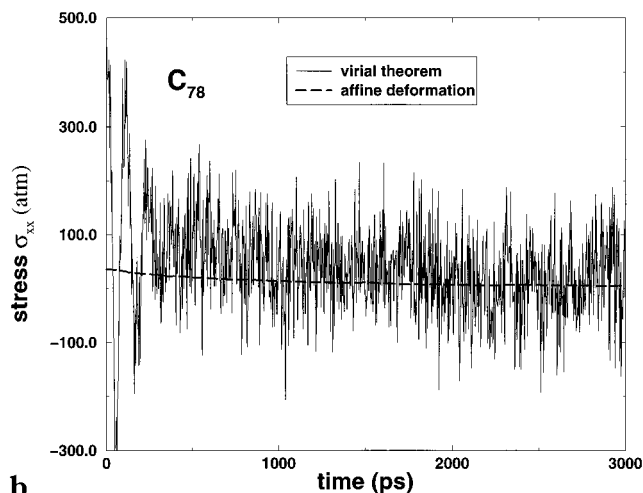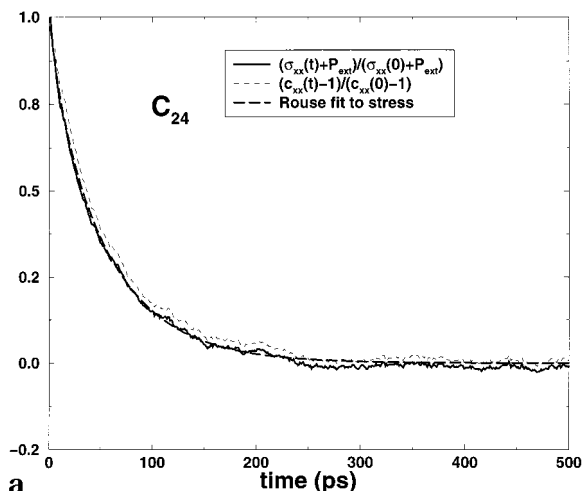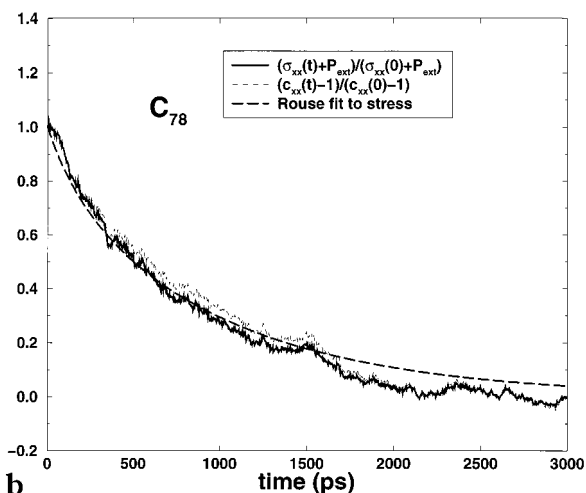
Figure 6. Evolution of the component σ_{xx} of the stress tensor with time t for (a) the C_{24} and (b) the C_{78} PE melt systems. The results at every time t have been obtained by applying either the virial theorem and averaging over all dynamical trajectories (thin solid line) or by using the thermodynamic expression, eq 25, as explained in the text (thick broken line). Simulation conditions: $T = 450$ K, $P_{ext} = 1$ atm.

Figure 7. Collected results for the evolution with time t of (i) the conformation tensor component $\tilde{c}_{xx}(t)$ as an average over all $NTL_x\sigma_{yy}\sigma_{zz}$ trajectories, and (ii) the stress tensor component σ_{xx}, calculated from $\tilde{c}_{xx}$ and $\partial(A/N_{ch})/\partial c_{xx}$ via eq 25 for (a) the C_{24} and (b) the C_{78} PE melt systems. Also shown in the figures are the best fits to the stress $\sigma_{xx}(t)$ according to the Rouse model, eq 14 in the text ($T = 450$ K, $P_{ext} = 1$ atm).

the relaxing configurations and averaging over all dynamical trajectories. The thick dashed line tracks the evolution of σ_{xx} as obtained from applying the thermodynamic stress equation, eq 25, based on the current values of $\tilde{c}_{xx}$ and $\partial A/\partial \tilde{c}_{xx}$, the latter taken from the melt elasticity simulations of ref 24. As expected, in both figures the estimates based on the virial theorem are subject to much higher statistical uncertainty, owing to the fluctuations in the instantaneous configurations. Clearly, averaging over many configurations is needed in order to improve the statistical quality of the virial theorem results. Apart from high-frequency noise, the virial theorem results display an oscillatory character similar to that of $L_y = L_z$, discussed in conjunction with Figure 3. When the noise and oscillations are smoothed out, the ensemble averaged stress $\sigma_{xx}(t)$ from the virial theorem is in very good agreement with the thermodynamic estimate obtained from $\tilde{c}_{xx}$ and $\partial(A/N_{ch})/\partial\tilde{c}_{xx}$. This is an important result, as it opens up the possibility of calculating stress with high precision directly from ensemble average conformational properties, based on a free energy function accumulated via efficient MC runs. The utility of eq 25 under transient conditions is demonstrated here for the first time. The transverse

components σ_{yy} and σ_{zz} fluctuate continuously around the constant value $-P_{atm}$, as required by the macroscopic restrictions placed on the $NTL_x\sigma_{yy}\sigma_{zz}$ ensemble, and are not displayed here.

5.5. Comparison to the Rouse Model Predictions. For the two systems studied, the curves showing the relaxation of the quantities $\tilde{c}_{xx}$ and σ_{xx} in the course of the $NTL_x\sigma_{yy}\sigma_{zz}$ runs, the latter quantity calculated from the thermodynamic expression, eq 25, are plotted collectively in parts a and b of Figure 7 for C_{24} and C_{78}, respectively. Also plotted in the same figures are best fits to $\sigma_{xx}(t)$ for the two model systems based on the Rouse model expression, eq 14. Two observations are important in parts a and b of Figure 7: First, the time scale for the relaxation of the quantities $\tilde{c}_{xx}$ and σ_{xx} is significantly smaller than the time scale characterizing the decay of the end-to-end vector autocorrelation function, $\langle\mathbf{R}(t)\cdot\mathbf{R}(0)\rangle/\langle R^2\rangle_0$, shown in parts a and b of Figure 4. According to the Rouse model predictions, eqs 14, 16, and 18, the dominant time governing the relaxation of $\tilde{c}_{xx}$ and σ_{xx} should be shorter than that governing the relaxation of $\langle\mathbf{R}(t)\cdot\mathbf{R}(0)\rangle/\langle R^2\rangle_0$ by a factor of 2. The simulation conforms closely to this prediction. Second, the fits to the stress relaxation function based on the

Table 2. Maximum Relaxation Time τ_R (ps), As Obtained from Fitting Eqs 14 and 16 to $NTL_x\sigma_{yy}\sigma_{zz}$ MD Results and Eq 18 to Equilibrium NVT MD Results ($T = 450$ K and $P_{ext} = 1$ atm)

MD method	quantity observed	C_{24}	C_{78}
$NTL_x\sigma_{yy}\sigma_{zz}$	$\dfrac{\tilde{c}_{xx}(t) - \tilde{c}_{xx}(\infty)}{\tilde{c}_{xx}(0) - \tilde{c}_{xx}(\infty)}$	115 ± 5	1950 ± 100
$NTL_x\sigma_{yy}\sigma_{zz}$	$\dfrac{\sigma_{xx}(t) - \sigma_{xx}(\infty)}{\sigma_{xx}(0) - \sigma_{xx}(\infty)}$	115 ± 5	2000 ± 100
equilib NVT	$\langle \mathbf{R}(t)\cdot\mathbf{R}(0)\rangle$	115 ± 10	2030 ± 100

Rouse model are indeed quite close. The same excellent comparison holds for the component $\tilde{c}_{xx}$ of the conformation tensor. Results from fitting the Rouse model expression to the quantity $\langle \mathbf{R}(t)\cdot\mathbf{R}(0)\rangle/\langle R^2\rangle_0$ under equilibrium conditions have been reported in our previous work.[20] Quantitative results from all three fittings are shown in Table 2, which presents the longest relaxation time τ_1 or Rouse time τ_R that best fits each one of the two curves in parts a and b of Figure 7 and the equilibrium curves in parts a and b of Figure 4 for the two PE melts simulated. To an excellent approximation, all estimates of τ_R are equal. This is a very significant result of the present work, because it shows that one can get the relaxation time spectra of an unentangled PE melt by performing $NTL_x\sigma_{yy}\sigma_{zz}$ MD simulations of stress relaxation on preoriented structures. Owing to the close relationship of $\tilde{c}$ and α with the $\mathbf{RR}$ tensor, observing their decay in the course of a transient nonequilibrium simulation leads to the relaxation spectrum in half the simulation time that is required to observe the decay of $\langle \mathbf{R}(t)\cdot\mathbf{R}(0)\rangle/\langle R^2\rangle_0$ under equilibrium or nonequilibrium conditions. The coincidence of relaxation time spectra between the current stress relaxation simulation and our earlier equilibrium MD runs on the same melts shows that the present stress relaxation MD simulations allow accessing the linear viscoelastic response of long-chain melts, which is practically impossible with previously applied nonequilibrium molecular dynamics methods.[9]

The efficiency of our $NTL_x\sigma_{yy}\sigma_{zz}$ method is expected to increase for longer chain, entangled PE melt systems, because the presence of entanglements should facilitate the return of the strained structures back to equilibrium. Consequently, the proposed methodology has the potential of alleviating the problem of long relaxation times characterizing PE melts of high MW, by significantly cutting down the CPU times relative to those required to track the evolution of the corresponding equilibrium systems. Of course, simulation of a large number of dynamical trajectories initiated at preoriented configurations is needed, but this is not a problem given the availability of multiprocessor parallel machines and of the EBMC algorithm.

5.6. The Shear Stress Relaxation Modulus $G(t)$. The shear stress relaxation modulus, $G(t)$, can be reconstructed from the values of τ_R obtained by mapping the simulation results to the Rouse model, using the equation[27]

$$G(t) = \frac{\rho RT}{M} \sum_{p:\text{all}} \exp\left(-\frac{2p^2 t}{\tau_1}\right) \qquad (26)$$

The results for the C_{24} and C_{78} chain systems simulated in this work are shown in Figure 8. The Rouse model describes mainly the terminal region and is not valid
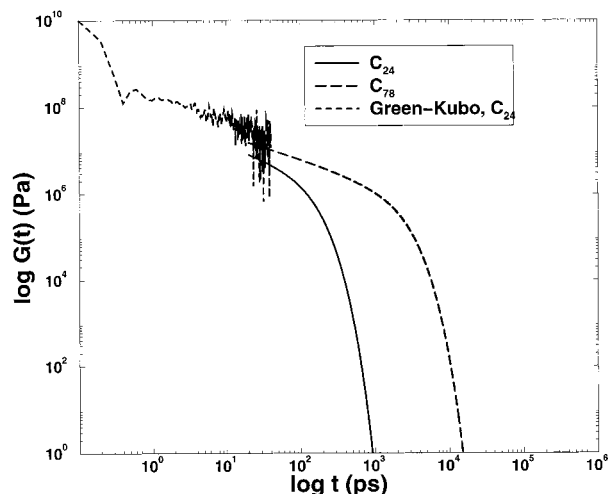
Figure 8. Relaxation modulus $G(t)$ for the C_{24} and the C_{78} PE chain systems. The curves have been reconstructed by using eq. 26 with the values of τ_R obtained by mapping the simulation results onto the Rouse model. $G(t)$ for C_{24}, as calculated directly from the Green–Kubo expression, is shown as a broken line on the left-hand side, short time region of the figure. ($T = 450$ K, $P_{ext} = 1$ atm).

for very short times. In Figure 8 , the curves based on eq 26 are shown for times longer than the relaxation time of a polymer segment of size equal to the Kuhn segment of a PE chain. A rough calculation shows that such a Kuhn segment consists of about 10 bonds, which suggests a relaxation time on the order of 20 ps.[42] This time is also consistent with the time needed for the full decorrelation of the torsional degrees of freedom of a PE chain at the same temperature.[20] The figure shows clearly that for times $t \geq 20$ ps the predicted $G(t)$ functions exhibit the usual Rouse behavior, characteristic of an unentangled system.

The shear stress relaxation modulus can also be calculated by using the relevant Green–Kubo equation. According to the latter, the zero-shear rate viscosity η_0 is given by the time integral of the time autocorrelation function of the off-diagonal components of the instantaneous stress-tensor:[41]

$$\eta_0 = \frac{V}{k_B T} \int_0^\infty \mathrm{d}t \langle \sigma_{\alpha\beta}(0)\sigma_{\alpha\beta}(t)\rangle \qquad (27)$$

By combining this with the equation

$$\eta_0 = \int_0^\infty G(t)\, \mathrm{d}t \qquad (28)$$

valid for an unentangled melt in the limit of linear viscoelasticity, we conclude that $G(t)$ can be estimated as

$$G(t) = \frac{V}{k_B T}\langle \sigma_{\alpha\beta}(0)\sigma_{\alpha\beta}(t)\rangle \qquad (29)$$

with $\alpha \neq \beta$. The instantaneous stress tensor in the above equations should be calculated by MD simulations from equilibrium (i.e., quiescent) conditions, by using the virial theorem. Because of the strong fluctuations in the values of the off-diagonal components of the instantaneous stress tensor, extremely long configurational averaging is required in order to calculate $G(t)$ accurately.[19] We have conducted a large number of equilibrium NVT MD runs for the C_{24} system, each for a

time period of about 1 ns, and the result for $G(t)$ obtained through eq 29, by applying also the technique of averaging over multiple time origins, is shown in Figure 8 by the dashed line. It is evident in the figure that the short time scale, Green–Kubo prediction for the evolution of $G(t)$ with t is above the curve obtained by the Rouse equation, corresponding to the regime of intermediate and long time scales. It is also evident that, within the statistical noise, the part of the curve following the typical Rouse behavior constitutes a smooth continuation of the part of curve obtained with the Green–Kubo relation. A further point to notice in Figure 8 is the value of $G(t)$ at time $t = 0$. This value is about 9.0×10^9 Pa, which is somewhat higher than the value of $G(t)$ (about 10^9 Pa) for a polymer in the glassy regime; it drops quickly to the value of 2×10^8 Pa over the time interval $0.1–1$ ps, beyond which it exhibits a weaker time dependence, quite similar to the one seen in our Rouse model-based predictions. The statistical noise of results for $G(t)$ obtained through the Green–Kubo relation makes it impossible to address reliably the regime $t > 10$ ps, which is most interesting from the point of view of rheological properties in the terminal region.

6. Conclusions

Prestrained PE melt configurations have been subjected to detailed atomistic MD simulations in the $NTL_x\sigma_{yy}\sigma_{zz}$ statistical ensemble. The preoriented configurations have been sampled with the end-bridging MC algorithm in the presence of an orienting field α_{xx}, representative of steady-state elongational flow at Deborah numbers smaller than 1. In the $NTL_x\sigma_{yy}\sigma_{zz}$ MD simulations, the field α_{xx}, which caused the polymer melt orientation during the EBMC calculations, is removed, and the return of the system back to equilibrium is monitored. Constraining the box length L_x in the x direction causes a gradual decrease of the stress component σ_{xx} down to its field-free equilibrium value $(-P_{\text{ext}})$. The physical experiment being simulated, therefore, is stress relaxation upon cessation of steady-state, uniaxial elongational flow.

Results have been presented for the temporal evolution of the stress component σ_{xx}, the diagonal components $\tilde{c}_{xx}$, $\tilde{c}_{yy}$, and $\tilde{c}_{zz}$ of the conformation tensor $\tilde{c}$, and the scaled end-to-end vector orientational autocorrelation function $\langle \mathbf{R}(t)\cdot\mathbf{R}(0)\rangle/\langle R^2\rangle_0$. All these results have been accumulated as configurational averages over many $NTL_x\sigma_{yy}\sigma_{zz}$ trajectories initiated at different prestrained configurations corresponding to the same value of α_{xx} for two model PE melt systems with uniform molecular weight distributions and polydispersity index 1.09: a 32-chain C_{24} and a 40-chain C_{78} melt.

The average stress σ_{xx} of the ensemble of relaxing configurations has been calculated as a function of time in two ways: via the molecular virial theorem, and via a thermodynamic expression involving the functional dependence of the Helmholtz energy upon the conformation tensor; the latter functional dependence has been determined previously through EBMC simulations of oriented melts. The two ways of calculating the stress yield consistent results, with the free energy-based expression being subject to much less statistical noise than the molecular virial expression. The utility of the thermodynamic expression is thus confirmed under (linear) nonequilibrium conditions.

By solving the appropriate Smoluchowski equation for the evolution of the time autocorrelation functions $\langle \mathbf{X}_p(t)\cdot\mathbf{X}_p(0)\rangle$ of the Rouse normal modes $\mathbf{X}_p$, $p = 0, 1, 2, \ldots$, subject to the initial conditions of the simulated relaxation experiment, analytical expressions have been derived for the time evolution of all three quantities σ_{xx}, $\tilde{c}_{xx}$, and $\langle \mathbf{R}(t)\cdot\mathbf{R}(0)\rangle/\langle R^2\rangle_0$. These analytical expressions provide an excellent description of the simulation results. By fitting the simulation results to the analytical expressions, the longest or Rouse relaxation time τ_R has been extracted for the two PE melts studied, the C_{24} and C_{78}. Identical values for the time τ_R are obtained from the relaxation of σ_{xx}, $\tilde{c}_{xx}$, and $\langle \mathbf{R}(t)\cdot\mathbf{R}(0)\rangle/\langle R^2\rangle_0$, which proves the internal consistency of the simulation results and the ability of the Rouse model to describe the viscoelastic properties of these two PE melts. Furthermore, the values of τ_R and the associated relaxation time spectra extracted from the relaxation simulations are identical to those determined in the past through equilibrium simulations of the same melts. This confirms that the present simulations have been carried within the linear regime.

The shear stress relaxation modulus $G(t)$ has been calculated from the equilibrium autocorrelation function of the instantaneous shear stress at short times and from the spectrum of relaxation times extracted by mapping the simulation results onto the Rouse model at long times. The two approaches yield consistent results and a shape of the $G(t)$ function typical of unentangled melts.

The simulation results and the Rouse analysis show that the relaxation of σ_{xx} and $\tilde{c}_{xx}$ takes place in a time scale shorter by a factor of 2 than the time characterizing the decay of the end-to-end vector orientational autocorrelation function $\langle \mathbf{R}(t)\cdot\mathbf{R}(0)\rangle/\langle R^2\rangle_0$ under equilibrium or nonequilibrium conditions. By reducing the CPU time required to capture the spectrum of relaxation times of long linear PE melts by a factor of 2, the present methodology helps alleviate the problem of long relaxation times, from which all equilibrium and nonequilibrium MD simulations of long-chain melts have suffered. By relying on the EBMC algorithm for generating large numbers of uncorrelated, oriented initial configurations and employing a precise thermodynamic expression of the stress cast in terms of the dependence of the free energy on coarse-grained structural variables, such as the conformation tensor, this method opens up the way toward the dynamic simulation of truly polymeric, entangled systems.

References and Notes

(1) Theodorou, D. N.; Suter, U. W. *Macromolecules* **1986**, *19*, 139.
(2) Argon, A. S.; Mott, P. H.; Suter, U. W. *Phys. Status Solidi B* **1992**, *172*, 193.
(3) Brown, D.; Clarke, J. H. *Macromolecules* **1991**, *24*, 2075.
(4) Gao, J.; Weiner, J. H. *Macromolecules* **1992**, *25*, 1348.
(5) Gao, J.; Weiner, J. H. *J. Chem. Phys.* **1992**, *97*, 8628.
(6) Gao, J.; Weiner, J. H. *Macromolecules* **1994**, *27*, 1201.
(7) Yang, L.; Srolovitz, D. J.; Yee, A. F. *J. Chem. Phys.* **1997**, *107*, 4396.
(8) Yang, L.; Srolovitz, D. J.; Yee, A. F. *J. Chem. Phys.* **1999**, *110*, 7058.
(9) Xu, Z.; de Pablo, J.; Kim, S. *J. Chem. Phys.* **1995**, *102*, 5836.
(10) Daivis, P. J.; Evans, D. J. *J. Chem. Phys.* **1995**, *103*, 4261.
(11) Todd, B. D.; Daivis, D. J. *J. Chem. Phys.* **1997**, *107*, 1617.

(12) Todd, B. D.; Daivis, D. J. *Int. J. Thermoplast.* **1998**, *19*, 1063.

(13) Todd, B. D.; Daivis, D. J. *Phys. Rev. Lett.* **1998**, *81*, 1118.

(14) Allen, M. P.; Tildesley, D. J. *Computer Simulation of Liquids*; Clarendon Press: Oxford, England, 1987.

(15) Evans, D. J.; Morris, G. P. *Statistical Mechanics of Nonequilibrium Liquids*; Academic Press: London, 1990.

(16) Morris, G. P.; Evans, D. J. *Mol. Phys.* **1985**, *54*, 629; *Phys. Rev. A* **1987**, *35*, 792. Evans, D. J.; Morris, G. P. *Mol. Phys.* **1987**, *61*, 1151; *Phys. Rev. A* **1988**, *38*, 4142.

(17) Todd, B. D. *Phys. Rev. E* **1997**, *56*, 6723; **1998**, *58*, 4587.

(18) Moore, J. D.; Cui, S. T.; Cohram, H. D.; Cummings, P. T. *Phys. Rev. E* **1999**, *60*, 6956.

(19) Mondello, M.; Grest, G. S. *J. Chem. Phys.* **1997**, *106*, 9327.

(20) Harmandaris, V. A.; Mavrantzas, V. G.; Theodorou, D. N. *Macromolecules* **1998**, *31*, 7934.

(21) Rouse, P. E. *J. Chem. Phys.* **1953**, *21*, 1272.

(22) Mondello, M.; Grest, G. S.; Webb, E. B.; Peczak, P. *J. Chem. Phys.* **1998**, *109*, 798.

(23) Pant, P. V. K.; Theodorou, D. N. *Macromolecules* **1995**, *28*, 7224.

(24) Mavrantzas, V. G.; Theodorou, D. N. *Macromolecules* **1998**, *31*, 6310.

(25) Mavrantzas, V. G.; Boone, T. D.; Zervopoulou, E.; Theodorou, D. N. *Macromolecules* **1999**, *32*, 5072.

(26) Ryckaert, J.-P.; Klein, M. *J. Chem. Phys.* **1986**, *85*, 1613.

(27) Doi, M.; Edwards, S. F. *The Theory of Polymer Dynamics*; Clarendon: Oxford, England, 1986.

(28) Mavrantzas, V. G.; Theodorou, D. N. *Comput. Theor. Polym. Sci.* **2000**, *10*, 1.

(29) Van der Ploeg, P.; Berendsen, H. J. C. *J. Chem. Phys.* **1982**, *76*, 3271.

(30) Dodd, L. R.; Theodorou, D. N. *Adv. Polym. Sci.* **1994**, *116*, 249.

(31) Ryckaert, J. P.; Bellemans, A. *Chem. Phys. Lett.* **1975**, *30*, 123.

(32) Edberg, R.; Evans, D. J.; Morriss, G. P. *J. Chem. Phys.* **1986**, *84*, 6933.

(33) Fixman, M. *Proc. Natl. Acad. Sci. U.S.A.* **1974**, *71*, 3050.

(34) Gō, N.; Scheraga, H. A. *Macromolecules* **1976**, *9*, 535.

(35) Nosé, S. *Mol. Phys.* **1984**, *52*, 255.

(36) Hoover, W. G. *Phys. Rev. A* **1985**, *31*, 1695.

(37) Theodorou, D. N.; Boone, T. D.; Dodd, L. R.; Mansfield, K. F. *Makromol. Chem. Theory Simul.* **1993**, *2*, 191.

(38) Allen, M. P. *Mol. Phys.* **1984**, *52*, 705.

(39) Harmandaris, V. A.; Mavrantzas, V. G.; Theodorou, D. N. Manuscript in preparation.

(40) Berendsen, H. J. C.; Postma, J. P. M.; van Gunsteren, W. F.; DiNola, A.; Haak, J. R. *J. Chem. Phys.* **1984**, *81*, 3684.

(41) Hansen, J. P.; McDonald, I. R. *Theory of Simple Liquids*; Academic Press: San Diego, CA, 1990.

(42) Exact values of the number of Kuhn segments making up a C_{24} or a C_{78} chain are given in ref 24. Also, the relaxation time of a chain segment equal to one Kuhn segment was calculated from (a) the relaxation time of the C_{24} PE melt, reported in ref 20 and (b) the number of monomers making up the Kuhn segment, by using that this time varies inversely proportionally with the square of the segment length in the unentangled regime.